Intercalibration of SUMER and CDS on SOHO. I. SUMER detector A and CDS NIS

Anuschka Pauluhn, Isabelle Rüedi, Sami K. Solanki, Jim Lang, C. Dave Pike, Udo Schühle, William T. Thompson, Jörg Hollandt, and Martin C. E. Huber

The results of an intercalibration between the extreme ultraviolet spectrometers Coronal Diagnostic Spectrometer (CDS) and Solar Ultraviolet Measurements of Emitted Radiation (SUMER) onboard the Solar and Heliospheric Observatory (SOHO) are presented. During the joint observing program Intercal_01, CDS and SUMER were pointed at the same locations in quiet Sun areas and observed in the same wavelength bands located around the spectral lines He I 584 Å, Mg X 609 Å, and Mg X 624 Å. The data sets analyzed here consist of raster images recorded by the CDS normal-incidence spectrometer and SUMER detector A and span the time from March 1996 to August 1996. Effects of the different spatial and spectral resolutions of both instruments have been investigated and taken into account in the analysis. We find that CDS measures generally a 30% higher intensity than SUMER in the He I 584-Å line, while it measures 9% and 17% higher intensities in Mg X 609 Å and Mg X 624 Å, respectively. Both instruments show very good temporal correlation and stability, indicating that solar variations dominate over changes in instrumental sensitivity. Our analysis also provides in-flight estimates of the CDS spatial point-spread functions.

OCIS codes: 120.5630, 120.6200, 300.6540.

1. Introduction

The Solar and Heliospheric Observatory[1] (SOHO) performs observations in the UV spectral domain with 6 of its 12 instruments. Frequently, 5 of them are used simultaneously to investigate common targets on the Sun. This implies the need, but also offers the possibility, to intercompare in orbit the radiometric calibration of these instruments. Such comparisons, particularly an evaluation of any change from the prelaunch laboratory calibration, are important, because solar UV instruments deployed in space have shown a degradation of their optics with time owing to a combination of contamination and radiation effects.[2–4] In fact in the past it has not often been possible to separate temporal changes in UV solar radiance from time-dependent changes in instrument sensitivity. Therefore a significant effort was made to avoid contamination during fabrication, assembly, and testing of the SOHO spacecraft and its instruments. Furthermore a careful radiometric laboratory calibration was performed, traceable to the primary synchrotron radiation standard.[5] Moreover the prelaunch calibration was supplemented by flights of calibration-rocket instruments, and, to maintain a valid radiometric calibration in orbit, the sensitivity of the relevant instruments was monitored regularly during the mission. We report here on the operational and scientific effort that was designed to assure the radiometric calibration of SOHO's instruments, namely, on multi-instrument, in-orbit calibration studies.

To validate the ground-based calibration and to assess any in-orbit changes, special joint observing programs (JOP's) have been designed and run regularly. The objective of the Intercal_01 JOP discussed in this paper is the radiometric cross-calibration of the SOHO instruments Solar Ultraviolet Measurements of Emitted Radiation (SUMER), Coronal Diagnostics Spectrometer (CDS), Ultraviolet Coro-

A. Pauluhn (pauluhn@astro.phys.ethz.ch), I. Rüedi, and S. K. Solanki are with the Institute of Astronomy, Eidgenössische Technische Hochshule-Zentrum, CH-8092 Zürich, Switzerland. A. Pauluhn is also with INTEC Bern. J. Lang and C. D. Pike are with the Rutherford Appleton Laboratory, Chilton, Didcot, Oxfordshire, OX11 0QX, United Kingdom. U. Schühle is with the Max-Planck-Institut für Aeronomie, D-37191 Katlenburg-Lindau, Germany. W. T. Thompson is with SM&A Corporation, NASA Goddard Space Flight Center, Code 682.3, Greenbelt, Maryland 20771. J. Hollandt is with Physikalisch-Technische Bundesanstalt, D-10587 Berlin, Germany. M. C. E. Huber is with the Department of Space Science, European Space Agency/European Space Research and Technology Centre, P.O. Box 229, 2200 AG Noordwijk, The Netherlands.

Received 25 May 1999; revised manuscript received 19 August 1999.

0003-6935/99/347035-12$15.00/0

nagraph Spectrometer, and Extreme-ultraviolet Imaging Telescope.

Besides pointing at the same location on the solar disk, several further requirements have to be fulfilled by the participating instruments during such an observation scheme: The coincident field of view must be sufficiently large to ensure good coregistration, yet must be small enough to be scanned relatively quickly. Suitable scans have been designed for the different raster schemes of the individual instruments by rastering over an extended area. In such rasters a spectrum is recorded at each spatial position. The actual target areas on the Sun were quiet regions, i.e., atmospheric regions marked by the absence of notable activity.

In this paper we present results of the interinstrument calibration between SUMER detector A and the long-wavelength band of the Normal-Incidence Spectrometer (NIS) of the CDS. Following a description of the individual data sets of each instrument and the corresponding data reduction (Section 2), we point out how the overlapping fields of view have been recognized and registered (Section 3) and present results of the comparison. Special emphasis is then put on investigation of the different spectral and spatial resolutions of the instruments (Section 4). Finally, the absolute radiances in the overlapping fields of view are compared (Section 5), and we conclude with a short summary of our findings (Section 6).

2. Data

A. Intercal_01 Joint Observing Program

For this first comparison between vacuum UV SOHO instruments we restricted the data set to the SUMER detector A and CDS NIS instruments. The preflight calibration has been performed independently for each instrument[6,7] in several selected wavelengths by comparison with a synchrotron light source (BESSY I, Berlin, Germany) by use of calibrated transfer sources.[5] The transfer sources were high-current hollow-cathode lamps equipped with a normal and a grazing-incidence collimator for, respectively, SUMER and CDS.

The spectral calibrations of both instruments were refined during the mission. For SUMER, observations of standard UV stars in the wavelength range above 1200 Å and observations of solar emission lines with known line ratios based on atomic physics were used.[8,9] For CDS an in-flight cross-calibration with a NASA/Naval Research Laboratories sounding rocket underflight was performed.[10] It turned out that alignment problems during the CDS preflight calibration limited the number of wavelengths at which the calibration could be unambiguously determined. Since the preflight and inflight data agreed at 584 Å, where the preflight data were known to be in good alignment, and since the in-flight measurements gave a wavelength-dependence curve whose shape agreed well with expectations, it was decided to base the CDS/NIS calibration on the in-flight measurements.

The overlap of the wavelength bands of SUMER and the CDS ranged from 513 to 633 Å. For the Intercal_01 JOP both instruments were pointed simultaneously at the same area at the solar disk center, which was chosen to be devoid of active or bright areas. Three emission lines in the common wavelength range, namely, He I at 584 Å and the two Mg X lines at 609 and 624 Å, were recorded. The data used for this investigation were taken during the period from March 1996 to August 1996. In the following we use notation 0325 as an abbreviation for 25 March 1996 etc. Although SUMER and CDS were pointing at the same region and scanned a similar area, the data sets obtained cannot be compared directly for the following reasons: There is uncertainty in the pointing of both instruments, the slit and pixel sizes (spectrally and spatially) of the two instruments are different, and possible step sizes for rastering are different as well. In addition, the two instruments do not have the same sensitivity; consequently the integration times had to be chosen accordingly for sufficiently large signal-to-noise (S/N) ratios to be achieved. This produces a different spatial sampling of the region, and the observing times of a particular point in the raster are generally not exactly simultaneous in the SUMER and CDS observations. Therefore a reliable comparison can be done only if the data of both instruments are resampled on a common spatial grid and spectrally integrated.

B. SUMER Data

SUMER is a stigmatic normal-incidence telescope/spectrograph operating in the range from approximately 500 to 1610 Å. Two orders of diffraction are observed in superposition, and the lines selected for this intercalibration with CDS are all observed in second order. The dispersion of the spectrometer varies slightly with wavelength and is around 44 mÅ/pixel in the first order and around 22 mÅ/pixel in the second order. The instrument is equipped with two detectors (A and B), each consisting of 1024×360 pixels. The data used for this study were obtained by detector A with a slit of angular dimensions of 1×300 arc sec^2. The instrument, its data acquisition, and its detector characteristics are described in Ref. 11. The SUMER rasters consisted of 80 steps with a step size of 0.76 arc sec and an exposure time t_{exp} of 16 s at each location. Combining all 80 single-slit images of one scan yields raster images of 60×300 arc sec^2 and a total accumulation time of 21.3 min. In the spectral dimension the available windows have 50 pixels for each line profile. Note that the two Mg X lines were recorded simultaneously by SUMER during this part of Intercal_01, whereas the He I line was observed in separate rasters.

Several detector-specific image correction routines have been applied (see, e.g., Ref. 8), such as a flat-field correction, a correction for the geometric image distortion, and a correction for the electronic dead time of the detector. Finally, the radiometric calibration was applied, converting the count rate per sampling

interval to radiance units (W m^{-2} sr^{-1}). Specifically, for the three lines of this intercalibration we used radiometric calibration factors $0.041736/t_{exp}$ W m^{-2} sr^{-1} per count for the He I line and $0.028433/t_{exp}$ W m^{-2} sr^{-1} and $0.024126/t_{exp}$ W m^{-2} sr^{-1} per count for the Mg X 609-Å and the Mg X 624-Å lines, respectively. Details about the SUMER radiometry can be found in Refs. 6, 9, and 12 and on the web pages http://www.linmpi.mpg.de/english/projekte/sumer/. The uncertainty of the calibrated images is 20%,[8,12] resulting mainly from uncertainties of the calibration source (7%), inhomogeneity of the optical system (8%), uncertainty of the ratio of the detector signal of the nominal slit and the calibration slit (5%), and finally uncertainty due to gain loss between voltage adjustments (10%).

Line fitting: The SUMER slit-image data from a given position in the spatial scans are in fact two-dimensional arrays, the first dimension being the wavelength, the second the spatial direction along the slit. The intensity distribution along the wavelength dispersion direction is in general best modeled by a Gaussian or a sum of Gaussian profiles in combination with an approximation of the background radiation. (The SUMER background is entirely continuum radiation measured in first order whereas the detector background is negligible. Note that this continuum is not present in the CDS measurements where the background stems from the detector.) Therefore Gaussian or multi-Gaussian profiles were fit to the spectra at each individual spatial location of the raster scans. The line-fitting algorithm is based on a least-squares method and was chosen to ensure consistency with CDS data preparation. Where possible, the results were compared with results produced by routines used for fitting the CDS data and showed very good agreement.

The He I 584-Å line could easily be fit by a single Gaussian with a constant background. In Fig. 1(a) is an example of such a fit for an arbitrary profile of the He I 584-Å line at a relatively bright point of the area.

The Mg X 609-Å line is situated on the wing of the H I Lyman-α 1215.7-Å line (Lα), and therefore a linear fit is necessary for background subtraction. In addition, several smaller maxima due to the presence of other spectral lines appear within the windows of both Mg X lines. Their elimination required fits with five Gaussian profiles. However, the S/N ratio at a single spatial position is not large enough to allow a reliable fit of this kind. Therefore we proceeded as follows. Every SUMER slit image was averaged over the 300 pixels along the slit. A multi-Gaussian fit to this average line profile was carried out. An example of a Mg X 624-Å line profile averaged along the slit and its fit is shown in Fig. 2. The parameters of the fit to the averaged profile were used as a first guess for the individual spectral fit of each spatial position along the slit; the background slope was kept fixed for all spatial points. Since the side peaks appearing in the averaged spectra are fairly well separated from the central spectral line of interest, only

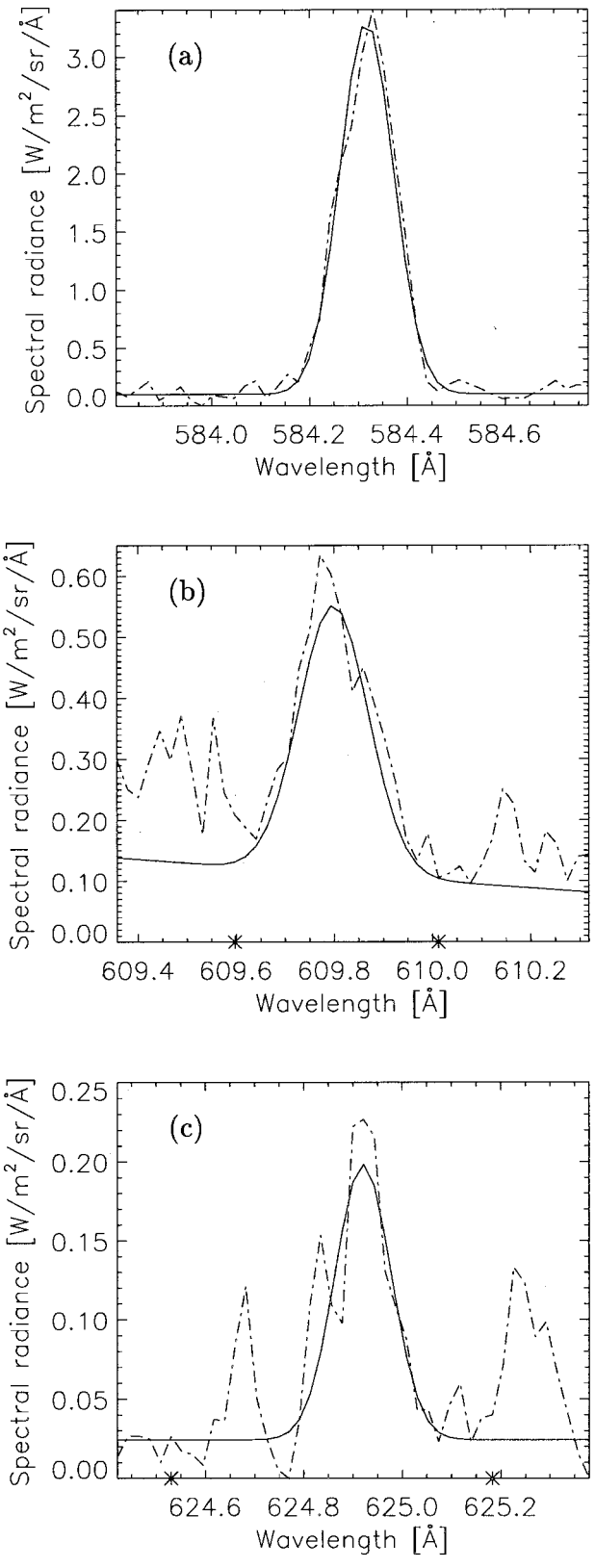

Fig. 1. Sample line profiles measured with SUMER (dash–dot lines) and the corresponding fit of a Gaussian plus a constant background (solid lines): (a) He I 584-Å line profile, (b) Mg X 609-Å line profile. The Mg X 609-Å line lies on the wing of H I Lα. (c) Mg X 624-Å line profile. In these examples the fit has been made between the pixels indicated by the asterisks. Lines lying nearby could be separated by the fit.

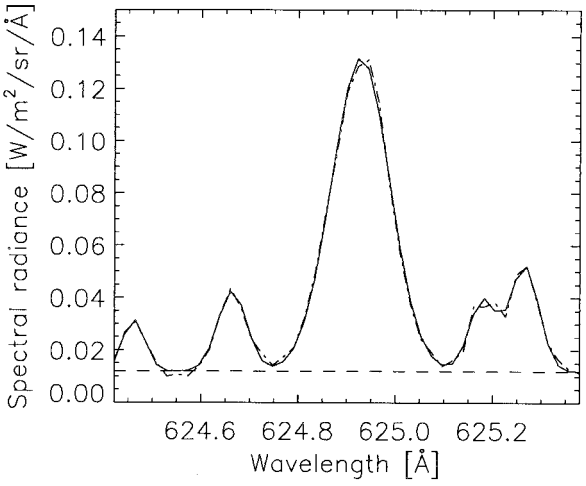

Fig. 2. Sample SUMER measurement of Mg X 624-Å line profile averaged along the slit (dash–dot line) and corresponding fit of five Gaussians plus a constant continuum background (solid line). The background is given by the dashed line.

the central portion of the spectral window was used for the fit to the nonaveraged profiles and was fit with a single Gaussian plus linear background. Blends from the first order (not present in the CDS measurements) can generally not be excluded in the SUMER lines in second order. Nevertheless they can be separated by observations with the two photocathodes of the SUMER detector, KBr and the bare microchannel plate, and have been determined to be less than 1% for the He I and Mg X lines.

Figures 1(b) and 1(c) show fits to the Mg X 609-Å line and the Mg X 624-Å line at a single spatial position, respectively.

The intensity images are then substituted by the radiances integrated over the spectral line profiles, given as the integral of the fit Gaussian curves, with the background subtracted. Let I_m be the value of the maximum of the Gaussian and dw its Doppler width (corresponding to $\sqrt{2}\sigma$ of the Gaussian). The radiances F are then calculated from the maximum and the width of the Gaussian as $F = I_m\sqrt{\pi}dw$.

C. CDS Data

The CDS instrument consists of a grazing-incidence telescope (Wolter-Schwarzschild Type II) that feeds two spectrometers, a normal-incidence stigmatic spectrometer (NIS) and a grazing-incidence spectrometer. The NIS has two toroidal concave gratings with different ruling densities mounted side by side and slightly tilted. They disperse two different wavelength bands one above the other onto the same detector.

The first wavelength band (NIS-1) ranges from 310 to 380 Å and the second band (NIS-2) from 517 to 633 Å. The data of JOP Intercal_01 reported here have been measured on NIS-2. The spectral pixel size of the CDS NIS ranges from 0.070 Å at 310 Å to 0.118 Å at 630 Å. Detailed descriptions of the instrument

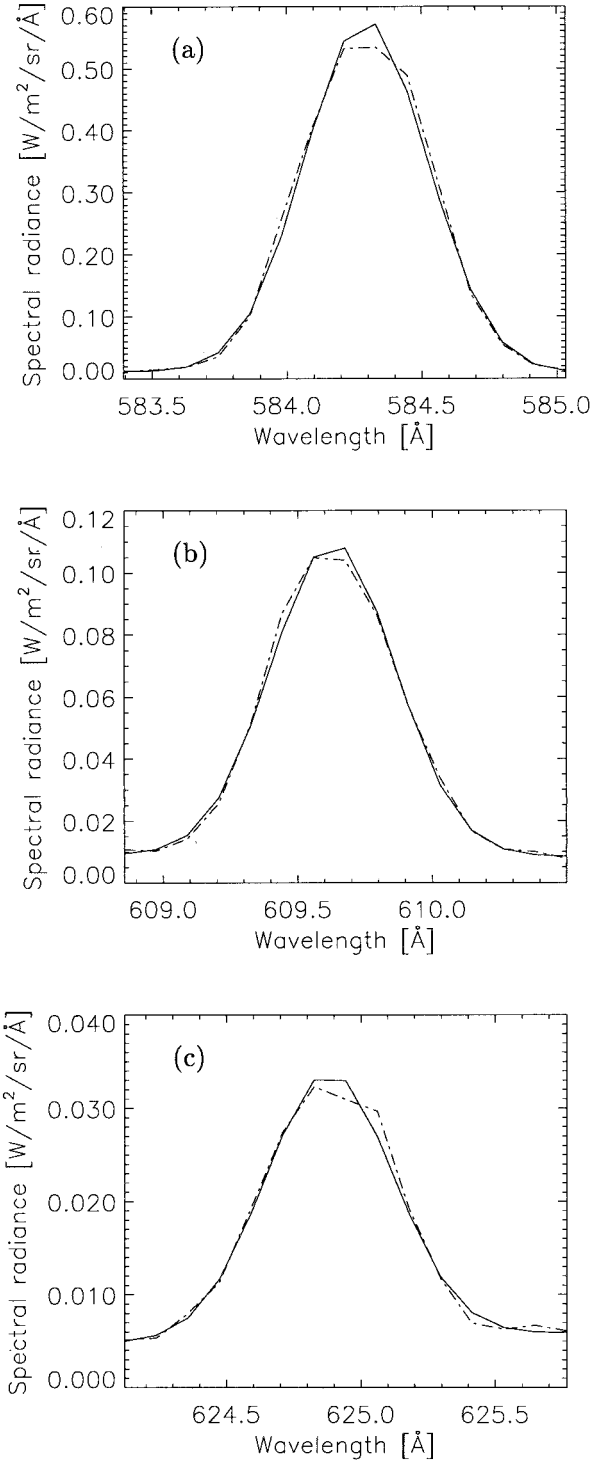

Fig. 3. Sample line profiles measured with CDS (dash–dot) and the corresponding fit of a Gaussian plus a constant background with ADAS (solid lines): (a) He I 584 Å, (b) Mg X 609 Å, (c) Mg X 624 Å.

and its data acquisition and handling systems can be taken from Refs. 13–15.

The data for the Intercal_01 JOP have been recorded by using the slit of angular dimensions 4 × 240 arc sec^2. Images are made by spatial rastering,

Table 1. Results of the Cross Correlation between CDS and SUMER Images

Date	Cross Correlation	x Width, y Width (arc sec)	x Shift, y Shift (arc sec)	Δt (min)
		He I (584 Å)		
0325	0.79	7.0, 7.5	(−9.12, −25)	1
0410	0.88	14.6, 13.6	(−1.52, 4)	4
0514	0.74	7.9, 15.9	(−6.84, −15)	10
0528	0.60	10.2, 8.5	(−6.08, −141)	10
0618	0.79	5.5, 8.7	(46.36, −7)	42
0816	0.75	9.9, 8.2	(−0.76, −21)	1
0826	0.83	9.8, 16.9	(0.76, −6)	4
		Mg X (609 Å)		
0325	0.65	8.0, 11.0	(−19.76, −26)	4
0410	0.90	15.0, 30.0	(−12.92, 4)	2
0514	—	—	—	—
0528	0.77	7.9, 8.9	(−13.68, −142)	4
0618	0.77	8.1, 13.0	(41.80, −9)	112
0816	0.68	14.6, 18.7	(−16.72, −19)	23
0826	0.83	9.5, 13.8	(−5.32, −4)	3
		Mg X (624 Å)		
0325	0.60	11.2, 19.3	(−19.76, −26)	4
0410	0.96	13.1, 30.0	(−12.92, 4)	2
0514	—	—	—	—
0528	0.75	8.2, 11.1	(−13.68, −142)	4
0618	0.76	10.6, 12.1	(41.80, −9)	112
0816	0.69	16.7, 30.0	(−16.72, −19)	23
0826	0.81	10.5, 13.1	(−5.32, −4)	3

i.e., by moving the slit perpendicular to its long axis in steps of 4 arc sec, thus producing 60 × 240-arc sec^2 raster scan images consisting of arrays of 15 (horizontal) by 143 (vertical) spatial pixels. The spatial pixel size along the slit corresponds to 1.68 arc sec. In the spectral dimension the available windows have only 15 or 21 points. The exposure time at each location was 80 s, resulting in a total accumulation time of 20 min for one raster. The main steps of the CDS data reduction consisted of correcting for burn-in and flatfielding. Details of the data reduction can be found in the CDS software notes available on the web pages on http://orpheus.nascom.nasa.gov/cds/. After applying CDS image-reduction routines the CDS intensities are obtained in units of counts per pixel per second, which are then converted to spectral radiance units. For the three lines of this intercalibration we used the radiometric calibration factors $0.016195776/t_{\mathrm{exp}}$ W m^{-2} sr^{-1} per count for the He I line and $0.017404872/t_{\mathrm{exp}}$ W m^{-2} sr^{-1} and $0.016980276/t_{\mathrm{exp}}$ W m^{-2} sr^{-1} per count for the Mg X 609-Å and the Mg X 624-Å lines, respectively. We applied the most recent radiometric calibration of the CDS NIS instrument, which is based on a comparison with sounding rocket data.[10] The main sources of uncertainty in the cross-calibration with the sounding rocket underflight are the absolute uncertainty in the sounding rocket measurements (12%) and the difficulty in isolating the line emission as seen by CDS with the lower spectral resolution sounding rocket data. Folding these effects together gives an uncertainty in the absolute calibration of 15% at 584 Å and 25% at 609 and 625 Å.

Line fitting: Gaussian line profiles have been fit by using the atomic data and analysis structure [(ADAS) originally developed by a JET joint undertaking].[16] The routine fits a Gaussian combined with a linear function for the background using a least-squares method.[17] Figure 3 shows examples of CDS spectra and their ADAS fit line profiles.

Finally, images corresponding to the total line radiation were obtained by integrating the Gaussian fit in exactly the same way as with the SUMER data.

3. Coregistration of SUMER and CDS Measurements

Seven data sets of quasi-simultaneous SUMER and CDS measurements were available for He I, and six were available for the Mg X lines.

Two-dimensional cross-correlation has been used to coregister the overlapping parts of the measured areas of the two instruments. For this purpose the CDS images (image size of 15 × 143 spatial points covering an area of 60 × 240 arc sec^2) have been resampled to match the spatial sampling of the SUMER images (image size of 80 × 360 spatial points covering an area of 60 × 360 arc sec^2), the new CDS

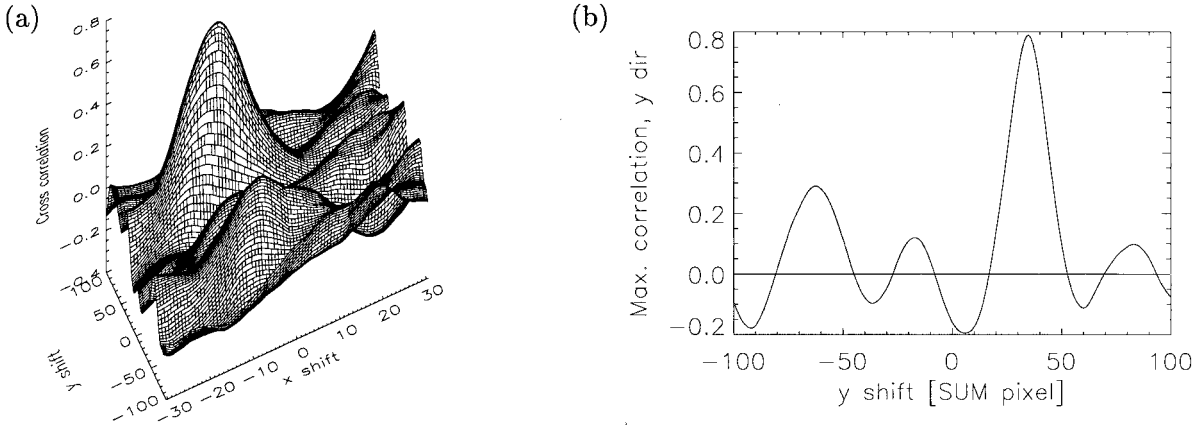

Fig. 4. Cross-correlation function of the SUMER and the CDS He I images recorded on 25 March 1996: (a) two-dimensional cross-correlation surface, (b) its profile through the maximum along the y direction.

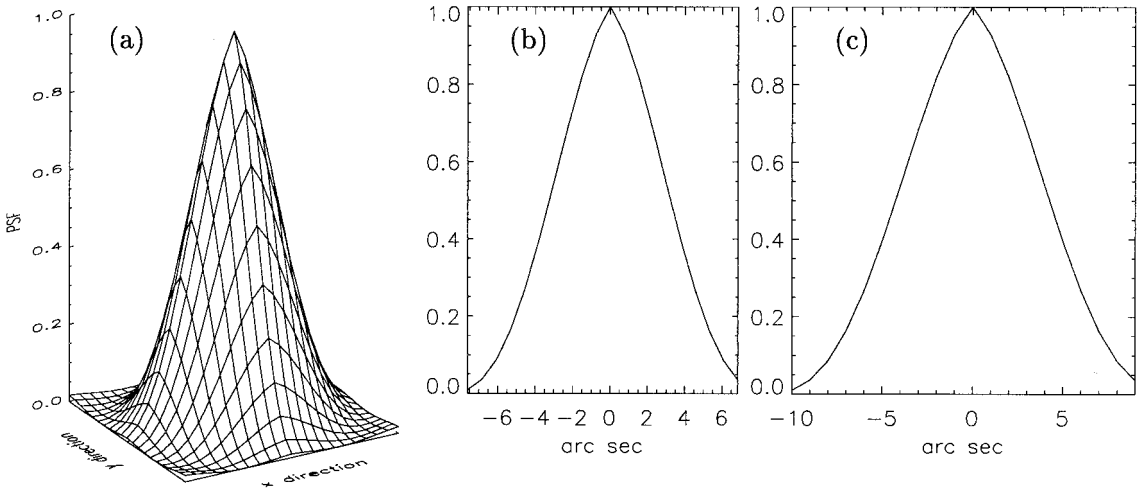

Fig. 5. Ellipsoidal Airy-like PSF used for convolution with the SUMER images: (a) surface plot on the SUMER grid; (b), (c) its profiles in the x and the y directions. This specific function corresponds to parameter $b = 0.31$.

images then consisted of 80 × 240 points. Subsequently the shifts of the CDS images relative to the SUMER images were calculated in the same spatial sampling units. The results are found in Table 1. In the first column are the dates of the observations (month and day in 1996), in the second column is the maximum cross-correlation of the patterns, in the third column are the (1σ-) widths of the cross-correlation function, in the fourth column are the corresponding shifts of the CDS image centers relative to the SUMER image centers, and in the last column are the temporal offsets of the start of the two measurements. The direction parallel to the slit is denoted the y direction, and its orthogonal is denoted the x direction.

Figure 4 depicts an example of such a two-dimensional cross-correlation function of a SUMER and CDS image. Figure 4(a) shows the cross-correlation surface of the He I images of 25 March 1996 (date 0325), and Fig. 4(b) shows the profile in the y direction through the maximum correlation value.

To cross-check the pointing of the two instruments, the center coordinates of the SUMER image (from the image header data) and the relative shifts of the images have been used to calculate the expected center coordinates of the CDS images (by using the results of the cross-correlation). These were then compared with the nominal ones. In most cases the pointings agreed within the instrumental uncertainties of ±10 arc sec for each instrument.

4. Spatial Resolution

The spatial resolutions of CDS and SUMER have been compared by using the He I data only, since they have the best S/N. For this purpose we degraded the resolution of every SUMER He I image, convolving it with a point-spread function (PSF) of increasing width. At each step we computed the cross-

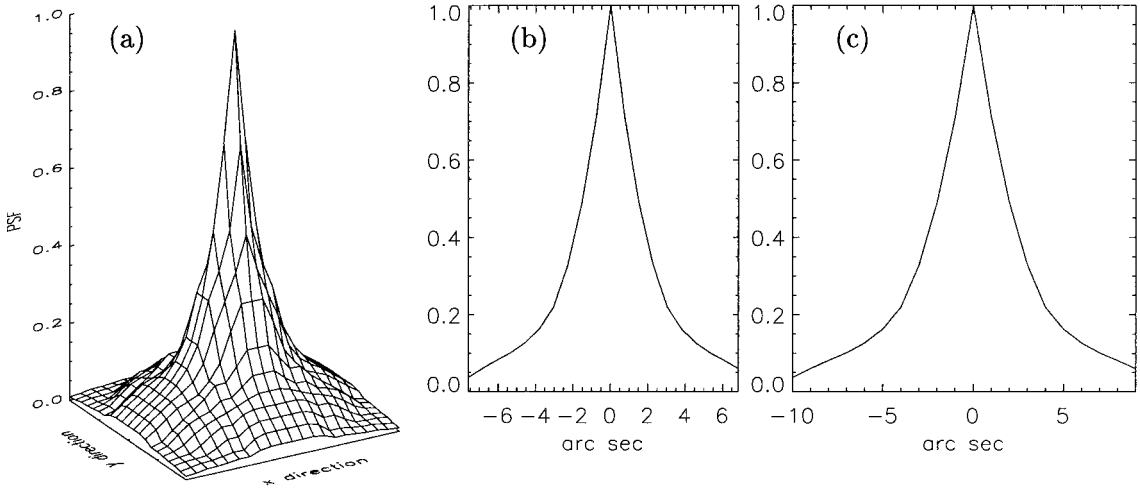

Fig. 6. Same as Fig. 5 but for the PSF similar to that plotted in Fig. 2 of Ref. 14.

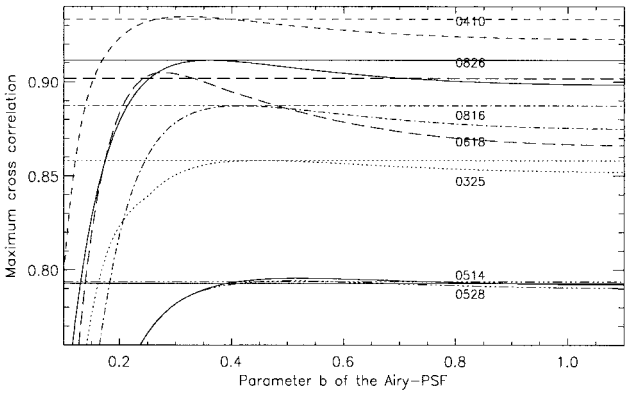

Fig. 7. Variation of the cross-correlation between the SUMER and the CDS image with the width of the Airylike PSF (width increasing toward lower b values). The horizontal lines designate the corresponding cross-correlation value calculated from convolution with the PSF shown in Fig. 6.

correlation with the CDS to determine the maximum of the cross-correlation coefficient. Two PSF's were used for this analysis. First, we started with a simple model of a rotationally symmetric PSF of a point source (see, e.g., Ref. 18, Chap. 3), defined by means of an Airy function:

$$PSF(r) = \frac{1}{\pi}\left[\frac{J_1(br)}{r}\right]^2,$$

where J_1 is a Bessel function of the first order. It was then modified to a slightly elliptical cross section (which was ~20% wider in the direction parallel to the slit than perpendicular to the slit) to take account of scattered light along the slit (see Fig. 5). Various widths of the PSF were tried by varying parameter b.

A good correlation was also achieved by convolution with a function similar in shape to the PSF given in Fig. 2 of Ref. 14. We used a symmetric function, as shown in Fig. 6, with a FWHM in the x and the y directions of 3.4 and 4 arc sec, respectively.

Figure 7 shows the variation of the cross-correlation coefficient between the SUMER and the CDS images with the width and the type of the PSF for all the available He I images. The horizontal lines depict the cross-correlation coefficients obtained by using the PSF similar to that of Ref. 14. The other curves show the cross-correlation coefficients obtained by using the Airy PSF and their variation as a function of parameter b. Both PSF models reach approximately a common maximum value. In the case of the Airy PSF, the optimum correlation is on average obtained for $b = 0.31$ (which corresponds to $\mathrm{FWHM}_x = 6$ arc sec, $\mathrm{FWHM}_y = 8$ arc sec). The much larger width (smaller b) suggested by the data set of 18 June (0618) may be explained by the rather large time lag of 42 min between the SUMER and the CDS measurements. Although the PSF derived from that of Ref. 14 has smaller FWHM values than the optimum Airy PSF, its wings extend rather far out and reach at least as far as the wings of the Airy PSF.

Figure 8 shows an example of the successive modifications of a SUMER image when it is transformed

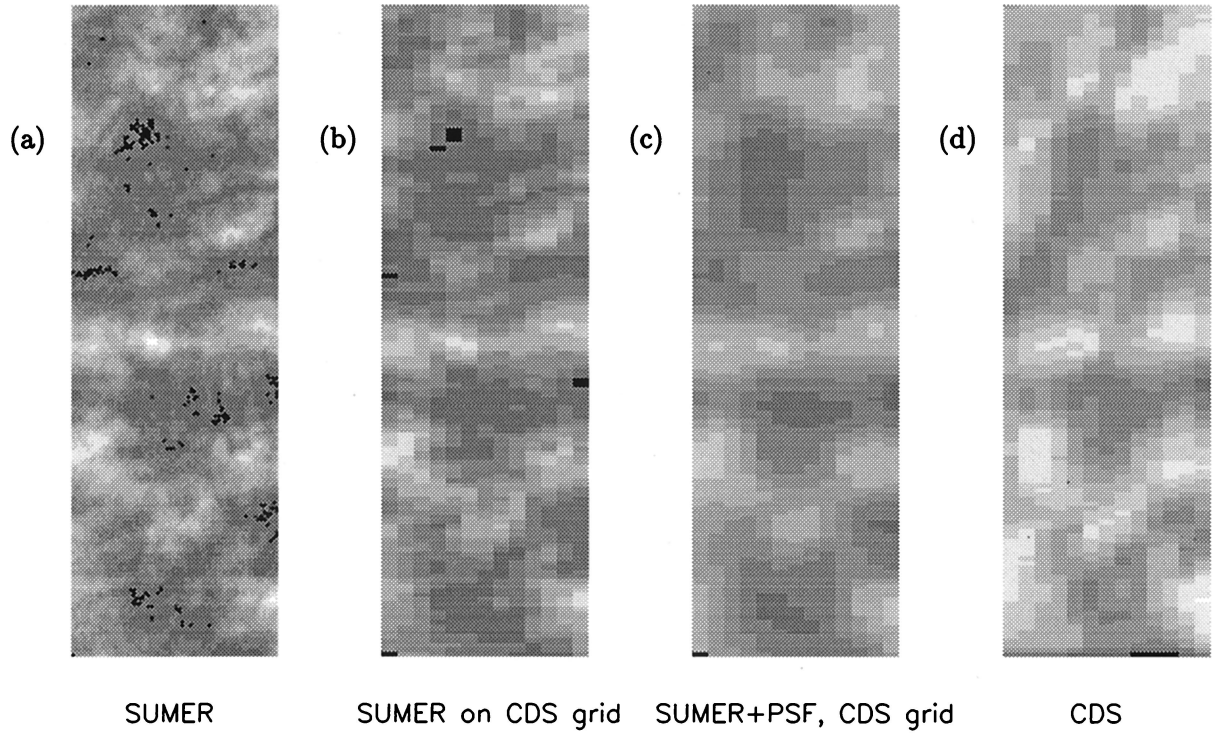

Fig. 8. Coaligned He I 584-Å images recorded by SUMER and CDS on 25 March 1996: (a) SUMER image, (b) SUMER image resampled to the CDS pixel size, (c) SUMER image additionally convolved with the PSF, (d) CDS image.

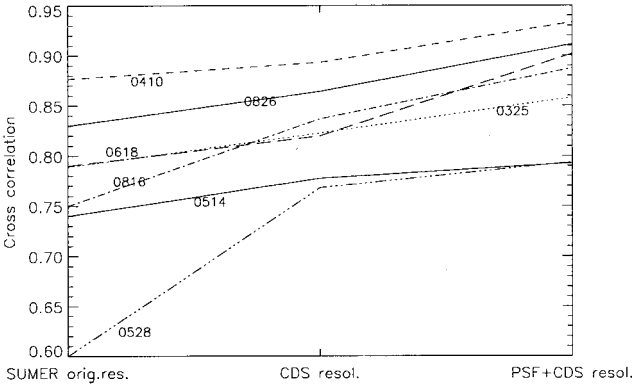

Fig. 9. Dependence of the cross-correlation coefficient of the SUMER and the CDS images on the resolution of the SUMER image.

so as to match the resolution of the corresponding CDS image. The leftmost image displays the original SUMER image. The next image exhibits the same image after it has been resampled at the CDS pixel size. The following image shows the SUMER image after resampling and convolution with the PSF from Fig. 6. The rightmost image shows the corresponding CDS image.

Figure 9 summarizes the cross-correlation coefficients obtained for all the He I data sets and for the following cases: (1) SUMER in the original resolution, (2) SUMER resampled to the CDS pixel size (improving correlation by 3–4%), and (3) SUMER resampled to the CDS pixel size and additionally convolved with the PSF of Fig. 6 (yielding a further increase in correlation by 3–4%).

Table 2. Regression Coefficients between SUMER and CDS from Scatter Plots for He I 584 Å (without PSF and with PSF Smoothing)

	Slope		Constant		One-Parameter Fit	
Date	No PSF	With PSF	No PSF	With PSF	No PSF	With PSF
0325	0.899	0.676	−0.105	0.006	0.654	0.696
0410	0.850	0.697	−0.108	0.006	0.666	0.714
0514	0.915	0.682	−0.142	−0.001	0.653	0.682
0528	0.782	0.590	−0.077	0.024	0.610	0.637
0618	0.908	0.586	−0.133	0.059	0.670	0.693
0816	0.837	0.593	−0.065	0.069	0.697	0.739
0826	0.889	0.682	−0.086	0.036	0.705	0.760
Average	0.869 ± 0.048	0.644 ± 0.051	−0.100 ± 0.031	0.028 ± 0.027	0.665 ± 0.031	0.703 ± 0.040
From Figs. 10/11	0.858	0.677	−0.094	0.014	0.668	0.646

Table 3. Regression Coefficients for Mg x 609 Å (without PSF and with PSF Smoothing)

	Slope		Constant		One-Parameter Fit	
Date	No PSF	With PSF	No PSF	With PSF	No PSF	With PSF
0325	0.999	0.732	−0.004	0.016	0.962	0.977
0410	0.823	0.764	0.004	0.014	0.878	0.909
0528	0.788	0.575	0.009	0.025	0.944	0.942
0618	0.733	0.552	0.018	0.033	0.962	0.974
0816	0.854	0.686	0.004	0.016	0.928	0.941
0826	0.856	0.661	0.004	0.021	0.927	0.949
Average	0.842 ± 0.008	0.659 ± 0.080	0.006 ± 0.007	0.020 ± 0.007	0.934 ± 0.031	0.949 ± 0.025
From Figs. 10/11	0.819	0.722	0.007	0.016	0.927	0.945

Table 4. Regression Coefficients for Mg x 624 Å (without PSF and with PSF Smoothing)

	Slope		Constant		One-Parameter Fit	
	No PSF	With PSF	No PSF	With PSF	No PSF	With PSF
0325	0.871	0.732	−0.001	0.003	0.824	0.840
0410	1.067	0.984	−0.007	−0.003	0.837	0.870
0528	1.040	0.720	−0.005	0.003	0.825	0.823
0618	0.804	0.673	−0.001	0.003	0.769	0.774
0816	0.967	0.835	−0.003	0.001	0.854	0.867
0826	0.859	0.678	−0.003	0.003	0.759	0.774
Average	0.935 ± 0.106	0.770 ± 0.120	−0.003 ± 0.002	0.002 ± 0.002	0.811 ± 0.038	0.826 ± 0.045
From Figs. 10/11	1.019	0.932	−0.006	−0.003	0.813	0.829

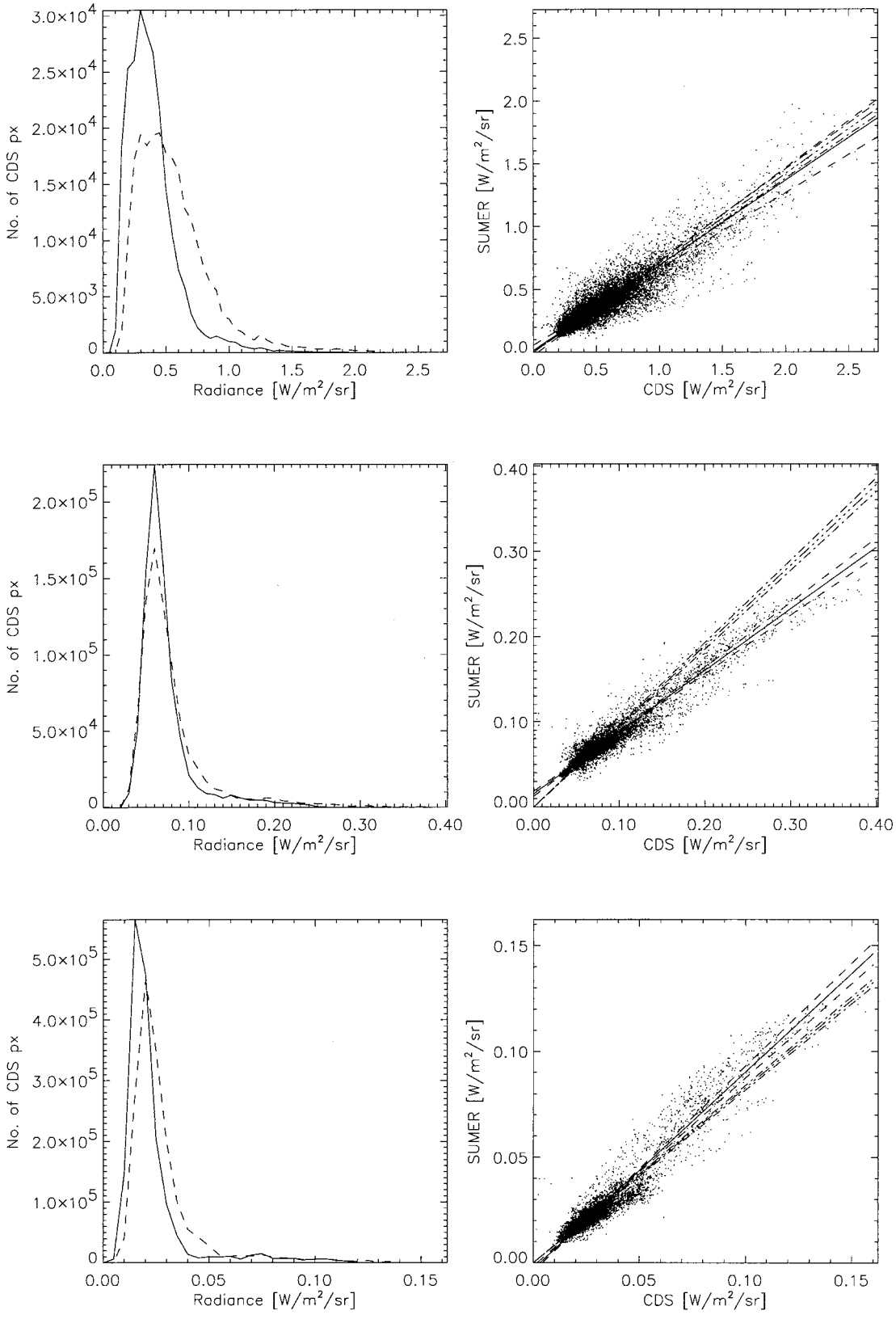

Fig. 10. Left: Histograms of the radiances of the overlapping fields of view for all data in He I 584 Å (upper plot), Mg X 609 Å (middle plot), and Mg X 624 Å (lower plot). The bin size was chosen to be 0.05 W m^{-2} sr^{-1} for He I 584 Å, 0.01 W m^{-2} sr^{-1} for Mg X 609 Å, and 0.005 W m^{-2} sr^{-1} for Mg X 624 Å. The histogram of the SUMER data is represented by the solid line, the histogram of the CDS data by the dashed line. Right: Scatter plots and linear regressions for the same data sets. The dashed lines represent the fitted curves for both regressions (SUMER versus CDS, CDS versus SUMER), and the solid line between represents their average. The dash–dotted lines represent the result from the one-parameter fit through the origin.

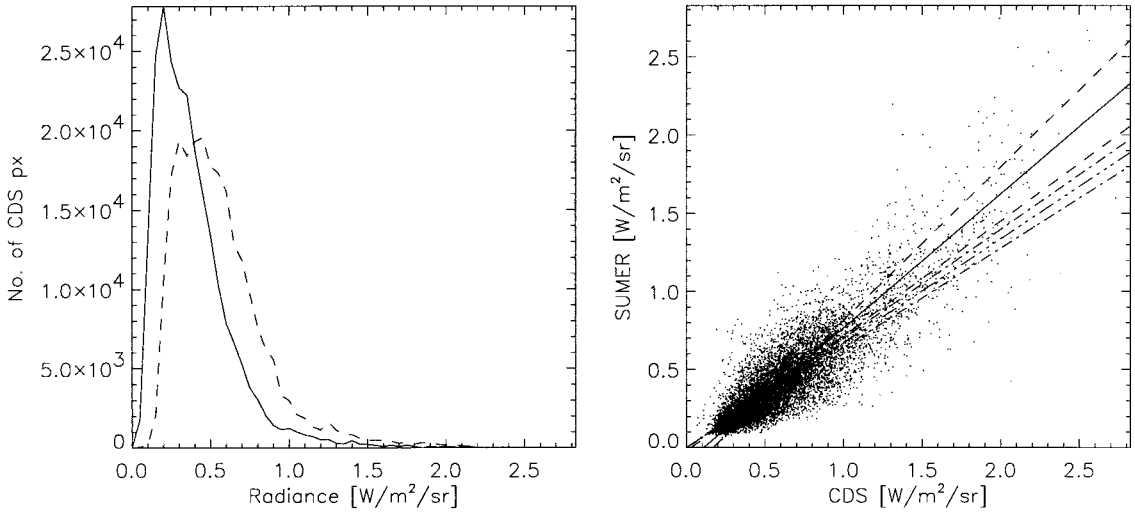

Fig. 11. Same as in Fig. 10 for He I 584 Å. Here the SUMER data have been resampled only to match the CDS grid but not convolved with a PSF.

5. Radiometric Intercalibration

To compare the absolute radiances in the overlapping areas, we used the SUMER images resampled to the CDS spatial sampling grid as well as the SUMER images resampled and convolved with the PSF from Fig. 6.

The intensity distributions from both instruments for all overlapping fields of view were plotted in histograms. Furthermore the intensities of the corresponding pixels were compared in scatter plots. Linear regression has been used to calculate the relationship between the SUMER and the CDS intensities. The fact that both variables are measurements, and consequently both have statistical uncertainties, was taken into consideration by carrying out two regressions between which dependent and independent variables were exchanged and computing the average of the fit parameters of both fits. All the fits were also repeated with the offset restricted to zero. Again both slopes (SUMER versus CDS and vice versa) were calculated, and the average of the slopes was computed. The results of all the linear fits characterizing the relation between the SUMER and the CDS measurements are given in Tables 2–4. We also combined all the images of one wavelength band to one large data set and computed the three histograms and scatter plots for these data. The results are shown in Fig. 10 for the SUMER images convolved with the PSF from Fig. 6, and the parameters of the fits are given in the last rows of Tables 2–4. As a comparison Fig. 11 depicts the histogram and the scatter plot for the He I 584-Å data but without convolution with a PSF. The dashed lines represent the fit curves for both regressions (SUMER versus CDS, CDS versus SUMER), and the solid line in between represents their average. The dash–dotted lines represent results from the one-parameter fit through the origin. The histograms show that the intensity distributions are shifted toward smaller values for the SUMER measurements. This is also indicated by the regression. The χ^2 errors of the fits range from the order of 10^{-2} for He I 584 Å to 10^{-4} and 10^{-5} for Mg X 609 Å and Mg X 624 Å, respectively, for both kinds of fit.

Figure 12 shows for each date the average radiance in the overlapping field of view for He I 584 Å, Mg X 609 Å, and Mg X 624 Å. For He I 584 Å the SUMER measurements are systematically lower than the CDS measurements by ~30%. In Mg X 609 Å and Mg X 624 Å a systematic offset of approximately 9% and 17% is observed, respectively. Also, the line ratios He I/Mg X are lower for SUMER than for CDS, which is not the case for the line ratios Mg X 609 Å/Mg X 624 Å. This could be induced by the different radiometric calibrations. The uncertainties shown in Fig. 12 represent the possible uncertainties due to the radiometric calibration of the two instruments only. The uncertainty resulting from the fitting and the background subtraction is negligible. It amounts to 8% for each single profile for the He I 584-Å line and to 10–15% for the Mg X 609-Å line and 20% for the Mg X 624-Å line, and the averages are formed from very large sample sizes. Nevertheless the fitting procedures may lead to systematic errors. This has been tested by fitting Gaussian or multi-Gaussian profiles to the averages of all CDS and SUMER spectra, respectively, in the overlapping areas. For all the CDS data and for the SUMER He I 584-Å and Mg X 609-Å data no significant differences were obtained, whereas for the Mg X 624-Å data the SUMER average radiances of the overlapping areas calculated in this manner were slightly higher, indicating a smaller background. These values for the SUMER data are indicated by dotted lines in Fig. 12.

Note that the temporal variations observed in

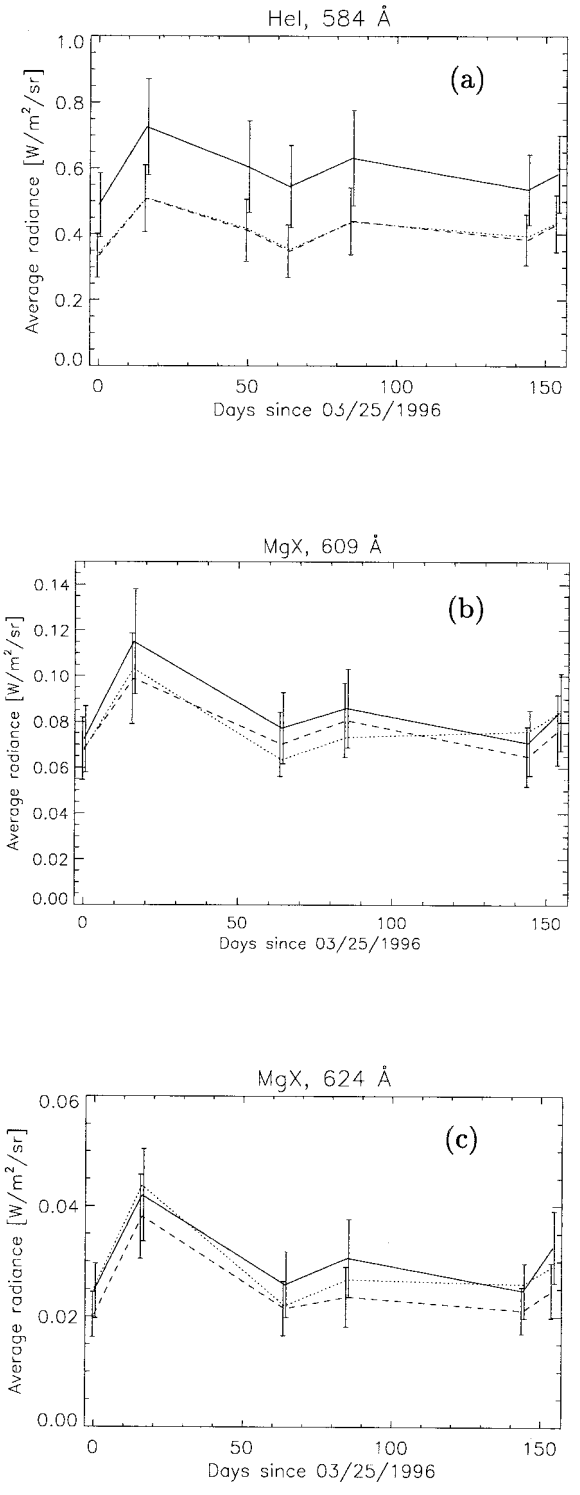

Fig. 12. Average radiances in the overlapping fields of view at all three wavelengths. The solid lines show the CDS measurements, and the dashed lines show the SUMER measurements. The error bars give the uncertainty from the radiometric calibration of the two instruments: (a) He I 584 Å, (b) Mg X 609 Å, (c) Mg X 624 Å. The dotted lines show the results for the SUMER radiance obtained from fitting a multi-Gaussian profile obtained by averaging all individual spectra in contrast to fitting the spectra at single positions and averaging afterward. The corresponding curves for the CDS data are not given here because they show very little difference from the solid ones.

SUMER and CDS are very similar for all three spectral lines. This strongly suggests that these variations are inherent solar variations and not due to instability in either instrument. Combining the temporal information obtained above with the fits to the scatter plots (Fig. 10) suggests that the linear regressions forced to pass through the origin are the most reliable for the He I data. They suggest a slope of 0.65–0.68 for the regression line. For the Mg X 609-Å data the fit when the smoothed SUMER data are used suggests a slope of approximately 0.66–0.72 and an offset of approximately 0.016–0.020, and for the Mg X 624-Å data a slope of around 0.77–0.93 and an offset of 0.002 are suggested. Nevertheless, taking into account that the data set of 10 April 1996 covers part of a coronal hole and its very bright boundary (it is this data set that extends the distributions in the Mg X lines toward unusual large values for quiet Sun conditions), and therefore neglecting its data, the suggested slope and offset are slightly different, namely, 0.70 and 0.003 for Mg X 624 Å, the fit of this smaller data set through the origin shows a slope of 0.82.

6. Results and Conclusions

For each of the three wavelength bands, He I 584 Å, Mg X 609 Å, and Mg X 624 Å, at least six data sets of simultaneous measurements of SUMER and CDS with overlapping fields of view were recorded between March 1996 and August 1996. Throughout this period the instrumental pointing was stable (within an uncertainty of ±10 arc sec given by each instrument), and both instruments showed reasonably good agreement in all three wavelength bands. A correlation analysis revealed that a large part of the differences in the pattern structure of the overlapping images can be ascribed to the different instrumental resolutions and raster designs. No significant variation of the correlation with time could be detected. A comparison of the absolute radiometric radiances yielded an offset of ~30%, with the SUMER instrument systematically measuring lower radiances than the CDS instrument in the He I line. In the Mg X 609-Å and 624-Å lines the SUMER measured 9% and 17%, respectively, lower radiances than CDS. Given the individual error estimates and uncertainties of both instruments of ±15–25% each, the agreement is good. At the present stage it is not possible to decide which instrument gives more accurate values since both their calibrations are equally reliable. For that purpose, data from other instruments would be required. Various such studies are either under way, such as comparisons between CDS and the Solar Extreme-UV Monitor (SEM) and between CDS and the Extreme-UV Imaging telescope (EIT), or planned, such as comparisons between SUMER and the UV Coronagraph Spectrometer (UVCS) and between SUMER and CDS/Grazing-Incidence Spectrometer (GIS). A comparison of a large portion of SUMER's spectrum with the solar spectrum obtained by the SOLSTICE experiment on the Upper Atmospheric

Research Satellite also suggests a small discrepancy toward lower intensities of the SUMER spectrum.[9] Both CDS and SUMER turned out to have very good radiometric stability since temporal changes occur simultaneously for both instruments.

A. Pauluhn and I. Rüedi were supported by the Programme de Dévelopment d'Experiences Scientifique (PRODEX) of the European Space Agency (ESA). We thank Klaus Wilhelm for the SUMER radiometry routine and for helpful comments on the manuscript. The SUMER project is financially supported by Deutsches Zentrum für Luft- und Raumfahrt (DLR), the Centre National d'Etudes Spatiales (CNES), the National Aeronautics and Space Administration (NASA), and the ESA PRODEX program (Swiss contribution). SOHO is a project of international cooperation between the ESA and NASA.

References

1. B. Fleck, V. Domingo, and A. Poland, eds., "The SOHO mission," Sol. Phys. **162,** Nos. 1–2 (1995).
2. M. C. E. Huber, A. K. Dupree, L. Goldberg, R. W. Noyes, W. H. Parkinson, E. M. Reeves, and G. L. Withbroe, "The Harvard experiment on OSO-6: Instrumentation, calibration, operation and description of observations," Astrophys. J. **183,** 291–312 (1973).
3. E. M. Reeves, J. G. Timothy, M. C. E. Huber, and G. L. Withbroe, "Photometric calibration of the EUV spectroheliometer on ATM," Appl. Opt. **16,** 849–857 (1977).
4. P. Lemaire, "Sensitivity changes in the CNRS Ultraviolet Spectrometer aboard OSO-8," ESA J. **15,** 238–242 (1991).
5. J. Hollandt, M. C. E. Huber, and M. Kühne, "Hollow cathode transfer standards for the radiometric calibration of VUV telescopes of the Solar and Heliospheric Observatory (SOHO)," Metrologia **30,** 381–388 (1993).
6. J. Hollandt, U. Schühle, W. Paustian, W. Curdt, M. Kühne, B. Wende, and K. Wilhelm, "Radiometric calibration of the telescope and ultraviolet spectrometer SUMER on SOHO," Appl. Opt. **35,** 5125–5133 (1996).
7. J. Lang, B. J. Kent, A. A. Breeveld, E. R. Breeveld, B. J. I. Bromage, J. Hollandt, J. Payne, C. D. Pike, and W. T. Thompson, "The laboratory calibration of the SOHO Coronal Diagnostic Spectrometer," Tech. Rep. RAL-TR-1999-036 (Rutherford Appleton Laboratory, Chilton, UK, 1999).
8. K. Wilhelm, P. Lemaire, U. Feldman, J. Hollandt, U. Schühle, and W. Curdt, "Radiometric calibration of SUMER: Refinement of the laboratory results under operational conditions on SOHO," Appl. Opt. **36,** 6416–6422 (1997).
9. U. Schühle, P. Brekke, W. Curdt, J. Hollandt, and P. Lemaire, "Radiometric calibration tracking of the vacuum-ultraviolet spectrometer SUMER during the first year of the SOHO mission," Appl. Opt. **37,** 2646–2652 (1998).
10. P. Brekke, W. T. Thompson, T. N. Woods, and F. G. Eparvier, "The EUV solar irradiance spectrum observed with the Coronal Diagnostic Spectrometer (CDS) on SOHO," submitted to Astrophys. J.
11. K. Wilhelm, W. Curdt, E. Marsch, U. Schühle, P. Lemaire, A. Gabriel, J.-C. Vial, M. Grewing, M. C. E. Huber, S. D. Jordan, A. I. Poland, R. J. Thomas, M. Kühne, J. G. Timothy, D. M. Hassler, and O. H. W. Siegmund, "SUMER-solar ultraviolet measurements of emitted radiation," Sol. Phys. **162,** 189–231 (1995).
12. K. Wilhelm, P. Lemaire, I. E. Dammasch, J. Hollandt, U. Schühle, W. Curdt, T. Kucera, D. M. Hassler, and M. C. E. Huber, "Solar irradiances and radiances of UV and EUV lines during the minimum of sunspot activity in 1996," Astron. Astrophys. **334,** 685–702 (1998).
13. R. A. Harrison and A. Fludra, eds., "The Coronal Diagnostic Spectrometer for the Solar and Heliospheric Observatory," Sci. Rep. SC-CDS-RAL-SN-95-0001, Vers. 6 (Rutherford Appleton Laboratory, Chilton, UK, 1995).
14. R. A. Harrison, E. C. Sawyer, M. K. Carter, A. M. Cruise, R. M. Cutler, A. Fludra, R. W. Haynes, B. J. Kent, J. Lang, D. J. Parker, J. Payne, C. D. Pike, S. C. Peskett, A. G. Richards, J. L. Culhane, K. Norman, A. A. Breeveld, E. R. Breeveld, K. F. Al Janabi, A. J. McCalden, J. H. Parkinson, D. G. Self, P. D. Thomas, A. I. Poland, R. J. Thomas, W. T. Thompson, O. Kjeldseth-Moe, P. Brekke, J. Karud, P. Maltby, B. Aschenbach, H. Bräuninger, M. Kühne, J. Hollandt, O. H. W. Siegmund, M. C. E. Huber, A. H. Gabriel, H. E. Mason, and B. J. I. Bromage, "The Coronal Diagnostic Spectrometer for the Solar and Heliospheric Observatory," Sol. Phys. **162,** 233–290 (1995).
15. R. A. Harrison, A. Fludra, C. D. Pike, J. Payne, W. T. Thompson, A. Poland, E. R. Breeveld, A. A. Breeveld, J. L. Culhane, O. Kjeldseth-Moe, M. C. E. Huber, and B. Aschenbach, "High resolution observations of the extreme ultraviolet Sun," Sol. Phys. **170,** 123–141 (1997).
16. H. P. Summers, "Atomic data and analysis structure," JET Joint Undertaking Rep. JET_IR(94)06 (Culham, UK, 1994); see also http://patiala.phys.strath.ac.uk/adas.
17. J. Lang, H. E. Mason, and R. W. P. McWhirter, "The interpretation of the spectral line intensities from the CHASE spectrometer on spacelab 2," Sol. Phys. **129,** 31–81 (1990).
18. M. Stix, *The Sun* (Springer-Verlag, Berlin, 1994), Chap. 3.